Aerosol Science 40 (2009) 16 – 28

Contents lists available at ScienceDirect

Aerosol Science

journal homepage: www.elsevier.com/locate/jaerosci

Comparison of analytical and CFD models with regard to micron particle deposition in a human 16-generation tracheobronchial airway model

Zhe Zhang[a], Clement Kleinstreuer[a,b,*], Chong S. Kim[c]

[a]Department of Mechanical and Aerospace Engineering, North Carolina State University, Raleigh, NC 27695, USA
[b]Department of Biomedical Engineering, North Carolina State University, Raleigh, NC 27695, USA
[c]Human Studies Division, National Health and Environmental Effects Research Laboratory, US EPA, Research Triangle Park, NC 27711, USA

ARTICLE INFO

Article history:
Received 28 March 2008
Received in revised form
20 August 2008
Accepted 26 August 2008

Keywords:
Human tracheobronchial airways
Computational analysis
Micron particle deposition
Deposition efficiency
Deposition fraction

ABSTRACT

A representative human tracheobronchial tree has been geometrically represented with adjustable triple-bifurcation units (TBUs) in order to effectively simulate local and global micron particle depositions. It is the first comprehensive attempt to compute micron-particle transport in a (Weibel Type A) 16-generation model with realistic inlet conditions. The CFD modeling predictions are compared to experimental observations as well as analytical modeling results. Based on the findings with the validated computer simulation model, the following conclusions can be drawn:

(i) Surprisingly, simulated inspiratory deposition fractions for the *entire* tracheobronchial region (say, G0–G15) with repeated TBUs in parallel and in series agree rather well with those calculated using analytical/semi-empirical expressions. However, the predicted particle-deposition fractions based on such analytical formulas differ greatly from the present simulation results for most *local* bifurcations, due to the effects of local geometry and resulting local flow features and particle distributions. Clearly, the effects of realistic geometries, flow structures and particle distributions in different individual bifurcations accidentally cancel each other so that the simulated deposition efficiencies during inspiration in a relatively large airway region may agree quite well with those obtained from analytical expressions. Furthermore, with the lack of local resolution, analytical models do not provide any physical insight to the air–particle dynamics in the tracheobronchial region.

(ii) The maximum deposition enhancement factors (DEF) may be in the order of 10^2 to 10^3 for micron particles in the tracheobronchial airways, implying potential health effects when the inhaled particles are toxic.

(iii) The presence of sedimentation for micron particles in lower bronchial airways may change the local impaction-based deposition patterns seen for larger airways and hence reduces the maximum DEF values.

(iv) Rotation of an airway bifurcation cause a significant impact on distal bifurcations rather than on the proximal ones. Such geometric effects are minor when compared to the effects of airflow and particle transport/deposition history, i.e., upstream effects.

© 2008 Elsevier Ltd. All rights reserved.

* Corresponding author at: Department of Mechanical and Aerospace Engineering, North Carolina State University, Raleigh, NC 27695, USA.
Tel.: +1 919 515 5261; fax: +1 919 515 7968.
E-mail address: ck@eos.ncsu.edu (C. Kleinstreuer).

0021-8502/$ - see front matter © 2008 Elsevier Ltd. All rights reserved.
doi:10.1016/j.jaerosci.2008.08.003

1. Introduction

Micron particle deposition in the tracheobronchial (TB) airways under normal inhalation conditions (say, inspiratory flow rate $Q = 15$–30 L/min), is of interest to toxicologists and regulators in case of toxic particulate matter as well as to health-care providers in case of bio-aerosols, radioactive and therapeutic particles (see review by Kleinstreuer, Zhang, & Donohue, 2008). While experimental deposition data sets are most valuable for gaining new physical insight and validating computer simulation models, it is the latter which allow for more realistic, detailed and less costly particle-deposition studies. Nevertheless, there are three challenging aspects when determining particle deposition in the human respiratory tract, i.e., the complex airway geometry, two- or three-phase flow simulation, and fluid–structure interaction. Computer modeling of the entire TB region, let alone the respiratory system, is still prohibitive. For example, considering the idealized lung model of Weibel (1963), there are 2^{15} branches for the 16th generation alone.

As a radically alternative approach, one-dimensional global airway systems have been constructed covering major respiratory zones or the entire lung. Classic examples are single- or multi-path models with analytical equations based on deposition calculations (Asgharian, Hofman, & Bergmann, 2001; Choi & Kim, 2007; Koblinger & Hofmann, 1990; NCRP, 1997; RIVM, 2002), and empirical correlations for total or regional depositions (ICRP, 1994; Kim & Hu, 2006; Kim & Jaques, 2004). While such greatly simplified systems can predict total micron particle depositions in the lung quite well, they also can be off by several factors at individual bifurcations (see Kleinstreuer, Zhang, & Kim, 2007).

A compromise solution to this complex problem in terms of computationally efficacy and realism has been proposed by Kleinstreuer and Zhang (2008). They divided the conducting zone, i.e., trachea (G0) to generation G15 into five intricately connected segments via adjustable triple-bifurcation units (TBUs). These TBUs extend "in series" as well as "parallel" after appropriate flow rate and geometry scaling, including out-of-plane branch orientation and branch asymmetry, in order to capture actual lung morphologies. Previous computational studies focused on specific TB segments, say, two or at most six bifurcations (for the most recent contributions see Li, Kleinstreuer, & Zhang, 2007; Longest & Xi, 2007; Zhang, Kleinstreuer, Donohue, & Kim, 2005; among others). The paper by Nowak, Kakade, and Annapragada (2003) gives the impression that they have already solved the problem of particle transport and deposition in the (entire) human lung. Specifically, their methodology of "3.5 generation subunit" used is quite different from what is presented in this paper. Their subunits are isolated, i.e., not interconnected for particle transport, assuming uniform particle distributions and averaged velocity profiles at the inlet of each subunit. Some other shortcomings of their paper include a lack of model validation, assumption of laminar flow, and ignoring the impact of head airways.

In this paper, the validated TBU model was employed to simulate in detail airflow as well as micron-particle transport and deposition in the TB airways. Deposition correlations for the entire TB tree are discussed as well.

2. Theory

2.1. Multi-level airway geometries

The TB region of 16 generations (i.e., G0–G15) is segmented into five levels, each represented by a TBU. These scaled TBUs extend in series and parallel in order to accommodate the TB tree (Fig. 1). Level by level, the TBUs can be adjusted to represent patient-specific lung morphologies with unique geometric features, such as asymmetric bifurcations, branches with partial occlusions and out-of-plane configurations to capture "subject variability", if so desired. In any case, air–particle outflow conditions of a representative oral airway model (Zhang et al., 2005) are taken as inlet conditions for G0, which at the G3 outlets are adjusted to become inlet conditions for G3–G6, etc. (see Fig. 1). Thus, multi-level adjustments include scaled geometric configurations and local flow field quantities, such as velocities, pressures and, if appropriate, turbulence parameters, as well as particle distributions and velocity profiles. The TBU dimensions are similar to the Weibel Type A geometries, assuming a lung volume of 3.5 L. The aerosol dynamics in the first TBU, i.e., G0–G3, compared well with simulation results obtained for a more realistic triple bifurcation (see Li et al., 2007). Uniform pressures were assumed at the outlets of the bifurcation units. But, the outlet tubes were extended to eliminate/reduce any outlet and downstream effects.

2.2. Airflow equations

For inhalation flow rates above 12 L/min turbulent flow may occur in the trachea and the first few bifurcations due to the laryngeal jet (Kleinstreuer & Zhang, 2003; Zhang & Kleinstreuer, 2004; among others). Various low-Reynolds number (LRN) turbulence models have been proposed (see Tian & Ahmadi, 2007; Zhang & Kleinstreuer, 2003a); however, as confirmed by Varghese and Frankel (2003) an adapted form of the LRN k–ω turbulence model of Wilcox (1998) is most appropriate for such internal laminar-to-turbulent flows. It does not require extra wall-layer functions, captures both flow regimes automatically, and produces sufficiently accurate results (Zhang & Kleinstreuer, 2003a).

All airflow equations as well as the necessary initial and boundary conditions are outlined in Zhang and Kleinstreuer (2003a, 2003b). For the assumed inhalation flow rate of 30 L/min, the flow field after bifurcation B6 for the present configuration is fully laminar (Kleinstreuer & Zhang, 2008).

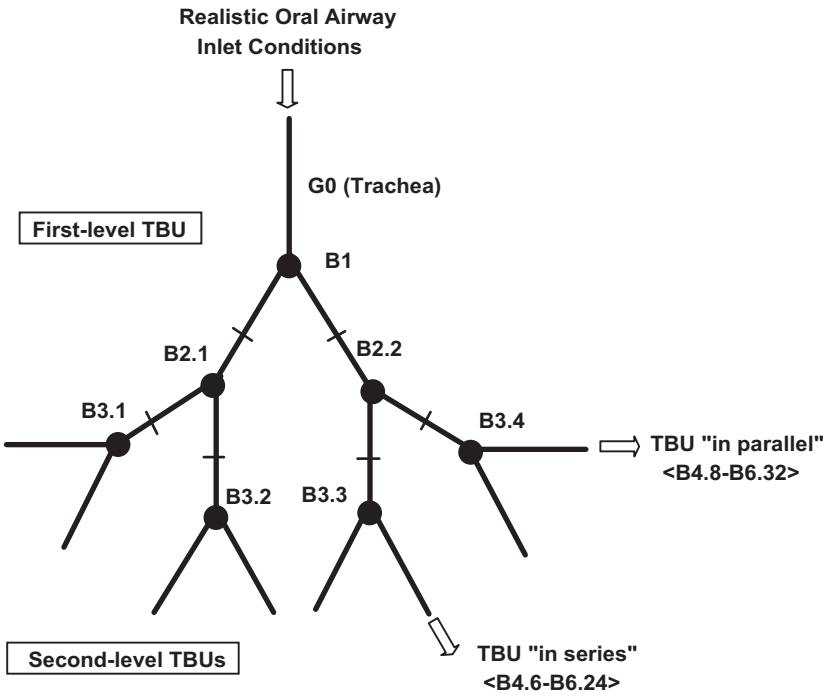

Fig. 1. Schematic of triple bifurcation units. B1—first bifurcation, B2.1 and B2.2—second bifurcation, B3.1, B3.2, B3.3 and B3.4—third bifurcation (the short cross lines indicate the segmental boundaries).

2.3. Micron particle transport equations

For any given inlet concentration of typically non-interacting, effectively spherical aerosols, a Lagrangian frame of reference for the trajectory computations of the micron particles ($d_p \geqslant 1\,\mu m$), can be employed. In light of the large particle-to-air density ratio, dilute particle suspensions, negligible particle rotation and Brownian motion and small thermophoretic forces, drag and gravity are considered as the dominant point forces away from the walls. Hence, the trajectory equation can be written as (Kleinstreuer, 2003, 2006):

$$\frac{d}{dt}(m_p u_i^p) = \frac{1}{8}\pi\rho d_p^2 C_{Dp}(u_i - u_i^p)|u_j - u_j^p| + m_p g_i \tag{1}$$

where ρ is the air density; u_i^p, m_p and d_p are the velocity, mass and diameter of the particle, respectively; g_i is the gravitational acceleration; and C_{Dp} is the drag force coefficient given by

$$C_{Dp} = C_D/C_{slip} \tag{2}$$

where C_{slip} is the slip correction factor (Clift, Grace, & Weber, 1978) and

$$C_D = \begin{cases} 24(1 + 0.15\,Re_p^{0.687})/Re_p & \text{for } 0.0 < Re_p \leqslant 1000 \\ 0.44 & \text{for } 1000 < Re_p \end{cases} \tag{3}$$

The particle Reynolds number is

$$Re_p = \rho|u_j - u_j^p|d_p/\mu \tag{4}$$

where μ is the fluid viscosity. In Eq. (1), u_i is the instantaneous fluid velocity with $u_i = \bar{u}_i + u_i'$, where $\bar{u}_i$ is the time-averaged or bulk velocity of the fluid, and u_i' are its fluctuating components. Traditionally, turbulence is assumed to consist of a collection of randomly directed eddies; hence, an eddy-interaction model (EIM) is used to simulate the particle trajectories, and the fluctuating velocities u_i' are obtained by (Gosman & Ioannides, 1981; Matida, Nishino, & Torii, 2000):

$$u_i' = \xi_i(\tfrac{2}{3}k)^{1/2} \tag{5}$$

where k is the turbulence kinetic energy; ξ_i are random numbers with zero-mean, variance of one, and Gaussian distribution. In the EIM, each particle is allowed to interact successively with various eddies and the random numbers are maintained constant during one eddy interaction while the corresponding turbulence intensities vary with the particle positions (Macinnes & Bracco, 1992; Matida et al., 2000). Each eddy has a lifetime t_E and length scale l_E given by

$$t_E = 1.5^{1/2} C_\mu^{3/4} \frac{k}{\varepsilon} = \frac{0.2}{\omega} \quad \text{and} \quad l_E = C_\mu^{3/4} \frac{k^{3/2}}{\varepsilon} = 0.164 \frac{k^{1/2}}{\omega} \tag{6a–d}$$

where C_μ ($= 0.09$) is a turbulence constant, ε is turbulence dissipation rate and ω is dissipation per unit turbulence kinetic energy. However, due to the assumption of turbulence isotropy, the fluctuating velocities normal to the wall calculated with Eq. (5) may be higher than the actual values (Kim, Moin, & Moser, 1987), which may overpredict the particle deposition in some cases (Matida, Finlay, Lange, & Grgic, 2004). As proposed by Matida et al. (2004), a near-wall correction can be used to simulate the near-wall particle trajectories, i.e., the component of fluctuating velocity normal to the wall u'_n can be expressed as

$$u'_n = f_v \xi (\tfrac{2}{3} k)^{1/2} \tag{7}$$

with

$$f_v = 1 - e^{-0.02 y^+} \tag{8}$$

where f_v is a damping function component normal to the wall considering the anisotropy of turbulence near the wall (Wang & James, 1999), y^+ is the non-dimensional wall distance, i.e., $y^+ = u_\tau y/\nu$ with u_τ being the friction velocity at the nearest wall, y being the distance to the nearest wall and ν being the local kinematic viscosity of the fluid. Usually, Eq. (8) is used for $y^+ < 10.0$, while $f_v = 1$ elsewhere.

2.4. Deposition parameters

The regional deposition of micron particles in human airways can be quantified in terms of the deposition fraction (DF) or deposition efficiency (DE) in a specific region (e.g., oral airway, first, second and third bifurcations etc.); they are defined as:

$$\mathrm{DF}_{\mathrm{particle}} = \frac{\text{Number of deposited particles in a specific region}}{\text{Number of particles entering the mouth}} \tag{9}$$

$$\mathrm{DE}_{\mathrm{particle}} = \frac{\text{Number of deposited particles in a specifc region}}{\text{Number of particles entering this region}} \tag{10}$$

The relationship between the DE and DF at the TB region can be determined by the following equations:

$$\mathrm{DF}_{B_1} = \mathrm{DE}_{B_1}(1 - \mathrm{DE}_{\mathrm{oral}}) \tag{11a}$$

$$\mathrm{DF}_{B_2} = \mathrm{DE}_{B_2}(1 - \mathrm{DE}_{\mathrm{oral}})(1 - \mathrm{DE}_{B_1}) \tag{11b}$$

$$\mathrm{DF}_{B_i} = \mathrm{DE}_{B_i}(1 - \mathrm{DE}_{\mathrm{oral}})(1 - \mathrm{DE}_{B_1})(1 - \mathrm{DE}_{B_2}) \cdots (1 - \mathrm{DE}_{B_{i-1}}) \tag{11c}$$

Here, B_1, B_2, B_i are the first, second and ith bifurcation, respectively. It should be noted that all paralleled bifurcations are included for the bifurcation with a same number. For example, there are 2^{i-1} paralleled bifurcations for B_i.

In addition to the above two traditional deposition parameters DE and DF, a deposition enhancement factor (DEF) is considered to be employed to quantify local particle deposition patterns (Balashazy, Hofmann, & Heistracher, 2003; Zhang et al., 2005). The DEF is defined as the ratio of local to average deposition densities, i.e.,

$$\mathrm{DEF} = \frac{\mathrm{DF}_i / A_i}{\sum_{i=1}^{n} DF_i / \sum_{i=1}^{n} A_i} \tag{12}$$

where A_i is the area of a local wall cell (i), n is the number of wall cells in one specific airway region and DF_i is the local DF in the local wall cell (i). *Clearly, the presence of high DEF-values indicates inhomogeneous deposition patterns, including "hot spots" in terms of locally maximum particle depositions.*

The following common-used DE equations, as recommended by NCRP (1997), are employed to calculate the DE in the present airway geometries, i.e., for the analytical equation based mathematical modeling. It should be noted that the following Eqs. (13)–(15) were derived analytically for particle depositions in very simple geometries (e.g., straight circular tubes and bent tubes) with idealized inlet conditions (e.g., fully developed flow and uniform particle distribution).

Deposition by diffusion:

$$\mathrm{DE}_d = 1 - 0.819 e^{-14.63\Delta} - 0.0976 e^{-89.22\Delta} - 0.0325 e^{-228\Delta} - 0.0509 e^{-125.9\Delta^{2/3}} \tag{13}$$

where $\Delta = \pi \tilde{D} L / 4Q$ and $\tilde{D}$ is the particle diffusivity, L is the tube length, and Q is the volumetric flow rate.

Deposition by inertial impaction:

$$\mathrm{DE_i} = 1 - \frac{2}{\pi}\arccos(\beta St) + \frac{1}{\pi}\sin[2\arccos(\beta St)] \tag{14}$$

where β is the branching angle (in radians) and $St = \rho_\mathrm{p} d_\mathrm{p}^2 U/(18\mu \mathrm{D})$ with U being the mean velocity.

Deposition by sedimentation:

$$\mathrm{DE_s} = 1 - \exp\left(-\frac{4}{\pi}\frac{v_\mathrm{settling}}{U}\frac{L}{D}\cos\varphi\right) \tag{15}$$

where v_settling is the terminal settling velocity given as $v_\mathrm{settling} = C_\mathrm{slip}\rho_\mathrm{p} g d_\mathrm{p}^2/(18\mu)$, and φ is the inclination angle relative to gravity ($\varphi = 0$ degree for horizontal tube). Assuming that deposition mechanism is mutually exclusive, the total deposition efficiency DE can be given as (Goo & Kim, 2003):

$$\mathrm{DE} = \mathrm{DE_i} + \mathrm{DE_s} + \mathrm{DE_d} - \mathrm{DE_i DE_s} - \mathrm{DE_i DE_d} - \mathrm{DE_s DE_d} + \mathrm{DE_i DE_s DE_d} \tag{16}$$

3. Numerical methods

The numerical solutions of airflow transport equations with LRN k–ω model or laminar flow model, were carried out with a user-enhanced commercial finite-volume based program, i.e., CFX from ANSYS Inc. (2006). The numerical program uses a structured, multiblock, body-fitted coordinate discretization scheme. All variables, including velocity components, pressure, and turbulence quantities, are located at the centroids of the control volumes. An improved Rhie–Chow interpolation method was employed to obtain the velocity components, pressure and turbulence variables on the control volume faces from those at the control volume centers (ANSYS Inc., 2006). A Quadratic Upwind (QUICK) differencing scheme, which is third-order accurate in space, was used to model the advective terms of the transport equations (ANSYS Inc., 2006). The sets of linearized and discretized equations for all variables were solved using the Block Stone's method (ANSYS Inc., 2006).

The particle transport equation (Eq. (1)) was solved with an off-line F90 code with parallelized algorithms (Longest, Kleinstreuer, & Buchanan, 2004; Zhang et al., 2005). A second-order improved Euler predictor–corrector method (Longest et al., 2004) was then used for the integration of the particle trajectory equation, including turbulent dispersion effects with near-wall correction (cf. Eqs. (5)–(8)). Particle deposition occurs when its center comes within a radius from the wall, i.e., local surface effects such as migration in mucus layers or resuspension due to clearing have been currently ignored. In the present simulations, 200,000 to 1,000,000 randomly selected, uniformly distributed particles were originally released at the mouth inlet. Considering the large loss of particles in the medium to the lower airway units, the particle inlet profiles at bifurcation units B7–B9, B10–B12 and B13–B15, were reconstructed to increase the amount of released particles. In this case, a certain amount of "daughter" particles were generated randomly in a circle around each "parent" particle, forming small "particle clouds". The radius of the small circle is about 5–10 times of the particle diameter and the distribution of daughter particles inside the circle is randomly uniform. The introduction of daughter particles has been tested to have negligible effects on actual particle deposition. That was deduced after finding that additional "parent" particles at the mouth inlet and upstream units had no measurable impact. In a word, particle deposition, including DE and DF, was tested to be independent of the number of particles released and particle cloud reconstructed.

The computational mesh was generated with CFX Build4 (ANSYS Inc., 2006), where the near-wall region requires a very dense mesh. Specifically, the thickness of the near-wall cells was chosen to fully contain the viscous sublayers and to resolve any geometric features present there. The mesh topology was determined by refining the mesh until grid independence of the solution of flow and mass fraction fields as well as particle deposition was achieved. The final mesh featured about 670,000 cells for a triple bifurcation airway unit. All computations were performed on an IBM Linux Cluster with 175 dual Xeon compute nodes at North Carolina State University's High-Performance Computing Center (Raleigh, NC) and local dual Xeon Intel 3.0 G Dell workstations (CFPD Laboratory, Department of Mechanical and Aerospace Engineering, NC State University). The solutions of the flow field were assumed to be converged when the dimensionless mass and momentum residual ratios were $< 10^{-3}$. Improving the convergence criteria to $< 10^{-4}$ had a negligible effect on the simulation results. Typical run times for the fluid flow simulations were approximately 60–100 CPU hours for one TBU under steady inhalation condition. Utilizing the converged flow field solution, the micron particle trajectory simulations required approximately 20–80 CPU hours on four processors for each case simulated.

4. Model validations

The present computational fluid–particle dynamics (CFPD) model has been validated with various experimental data sets for steady and transient laminar flows in bifurcations (Comer, Kleinstreuer, & Zhang, 2001; Zhang & Kleinstreuer, 2002) and for laminar, transitional and turbulent flows in tubes with local obstructions (Kleinstreuer & Zhang, 2003; Zhang & Kleinstreuer, 2003a). Especially, the LRN k–ω model has been extensively validated and has been proven to be an applicable approach to capture the velocity profiles and turbulence kinetic energy for laminar-transitional-turbulent flows in the constricted tubes of

the upper airways (see Zhang & Kleinstreuer, 2003a). The current simulation approaches of micron particle deposition because of impaction and sedimentation, have been validated with both analytical solutions in straight pipes and experimental data for oral and double-bifurcation airway models (Kleinstreuer et al., 2007; Zhang et al., 2005; Zhang, Kleinstreuer, & Kim, 2002). A comparison of micron particle deposition in the present airway model with in vivo deposition data as a function of the particle aerodynamic diameter is given in Section 5.1.

In summary, the good agreements between experimental observations and theoretical predictions instill confidence that the present computer simulation model is sufficiently accurate to analyze airflow and particle transport/deposition in three-dimensional TB airways.

5. Results and discussion

5.1. Comparisons of TB DFs

One key validation approach for computer simulations is a comparison between predicted TB deposition and experimental measurements, as shown in Fig. 2. The TB DF is defined here as the number ratio of deposited particles in the entire TB region (i.e., G0 to G15, or B1–B15 for simulations) to the incoming particles at the mouth inlet. Considering the asymmetric airflow and particle distributions after the first TBU B1–B3, simulations of particle deposition in all subsequent TBUs in the lower airways are almost impossible (e.g., there are 2048 paralleled TBUs for B13–B15). Hence, we tracked the selected representative parallel TBUs (e.g., the TBUs which feature the highest and lowest flow rates), and then calculated the average deposition in the parallel bifurcation units to obtain the total TB deposition (see Fig. 2). The branch-averaged DFs were obtained from the specific correlations for each bifurcation "in series" in terms of the data for the representative "parallel" bifurcations. Of interest is that variations of simulated DFs in the TB region, as a function of particle diameter, are consistent with the experimental studies, and the simulation results essentially fall into the uncertainty bars for in vivo measurements (see Fig. 2). This confirms that the current CFPD modeling results, relying on the new TBU methodology, are sufficiently accurate.

The TB deposition may increase for micron particles as their diameters increase from 1 to 10 μm with $Q = 15$ L/min or from 1 to 7 μm with $Q = 30$ L/min, due to the increasing impaction (see Fig. 2). The higher the inhalation flow rate, the higher is the deposition of micron particles. Clearly, particles with $d_p \geqslant 7$ μm and $Q \geqslant 30$ L/min deposit either in the oral airway or in the TB region; they do not reach the alveolar region because of high inertial impaction. However, the TB DFs may decrease for large micron particles with high flow rates (e.g., $d_p \geqslant 10$ μm and $Q = 30$ L/min) because of enhanced uptake in the oral airway.

Comparisons between CFPD simulations and "mathematical modeling", i.e., results obtained with analytical and/or semi-empirical correlations are depicted in Fig. 3. In the mathematical modeling framework, the DFs in the oral airway are assumed to be the same as those in the CFPD simulations in order to have comparable starting points. The commonly used DE equations (13)–(16) were employed to calculate the DE for the present airway geometries. Clearly, considering the *total deposition* in the TB region, the CFPD simulations and mathematical modeling results agree astonishingly well, i.e., the relative errors are only

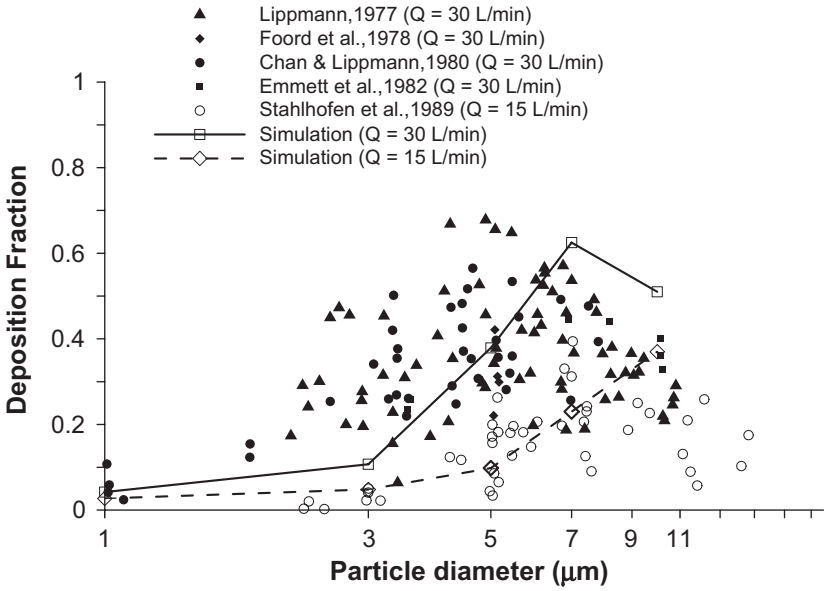

Fig. 2. Comparison of inspiratory TB deposition fractions between the present simulations and experimental measurements at different inspiratory flow rates Q (Chan and Lippmann, 1980; Emmett, Aitken, & Hannan, 1982; Foord, Black, & Walsh, 1978; Lippmann, 1977).

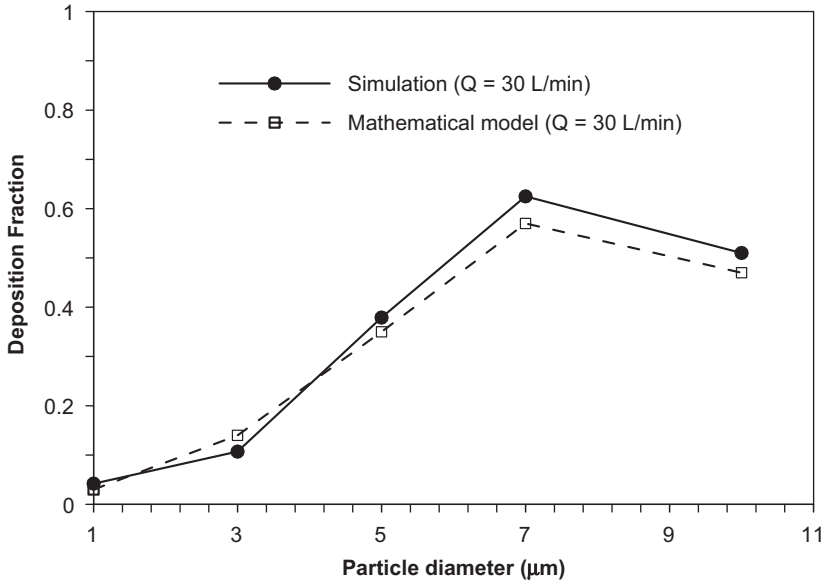

Fig. 3. Comparison of inspiratory TB deposition fractions between CFPD simulations and mathematical modeling at inhalation flow rate $Q = 30$ L/min.

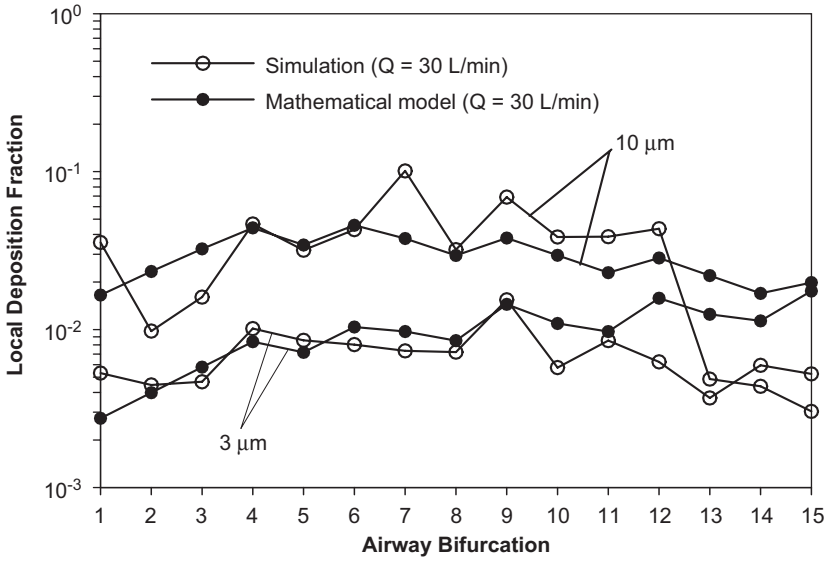

Fig. 4. Comparison of bifurcation-by-bifurcation deposition fractions of micron particles during inspiration between CFPD simulations and mathematical modeling based on Eqs. (13)–(16).

between 2.5% and 26%. However, on a local airway basis significant discrepancies appear. Specifically, Fig. 4 shows comparisons between CFPD simulation and mathematical modeling results for DFs of 3 and 10 μm particles at each bifurcation. It is shown that at some local bifurcations, for example, bifurcations B2, B3, B7, and B9, the mathematically predicted DF-values for 10 μm particles may differ greatly from the CFPD simulated data. This is due to the effects of local geometric features, and resulting local airflow structures and particle distributions as well as upstream deposition, recalling that the analytical DE-equations (see Eqs. (13)–(16)) were derived from particle transport in simple geometries (e.g., straight tubes) with idealized inlet flow profiles and particle distributions. The relative difference between numerical modeling and mathematical calculations can be as large as a few hundred percent at selected bifurcations. This indicates that the effects of geometry, flow structure and particle distributions at local bifurcations may cancel each other so that the simulated DFs in a relatively large airway region (e.g., the entire TB region) may agree well with that obtained from mathematical modeling.

From simulated results in Fig. 4 it can be also observed that the deposition of 10 μm particles at $Q = 30$ L/min mainly occurs at the large to medium-size airways (say, from mouth the generation G12 or bifurcation B12), while 3 μm particles still penetrate

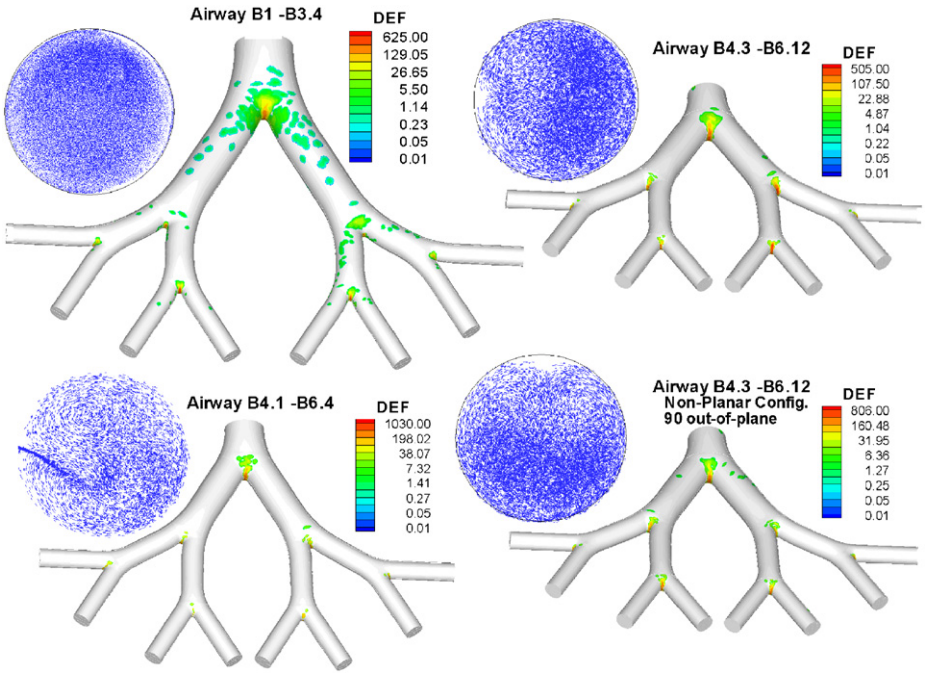

Fig. 5. Distributions of particle deposition enhancement factor (DEF) ($Q = 30$ L/min and $d_p = 5\,\mu$m). The cross-sectional views of particle distributions and direction vectors at the inlet of each airway unit are also shown. The mean areas of the surface element for calculating DEF are 0.2 and 0.05 mm^2 for airway units B1–B3 and B4–B6, respectively.

deeper into the lung. In general, the variations of local DFs for micron particles from B1 to B15 as a function of serial number (bifurcation levels) are complicated due to the mutual interactions among local airflow, particle distribution as well as particle deposition mechanisms. For example, the micron particle deposition due to impaction in small airways may decrease with the reduced flow rates, but the deposition due to sedimentation in these airways may increase with increasing residence time.

5.2. Local particle distributions and deposition patterns

Affected by the upstream deposition, local airflow and particle motion, micron particle distributions are non-homogenous and concentrations tend to be high in some areas (see Fig. 5). Specifically, at the oral and upper airways (e.g., trachea outlet), turbulent dispersion may randomize the cross-sectional particle distributions (see the inlet distribution at the TBU B1–B3.4). At the large airways (e.g., B4–B6), secondary flow mainly influences the cross-sectional particle distribution, and again inertial impaction is the dominant deposition mechanism. The distinct particle swirl motion can be observed at the inlets of the second-level TBUs (e.g., TBU B4.1–B6.4 and B4.3–B6.12), associated with the corresponding secondary vortices. At the small airways, the gravity angle may play a significant role on particle distribution due to the mechanism of sedimentation (e.g., fifth-level TBUs). Both gravitational settling and secondary motion lead to micron particle deposition in medium-sized airways (say, third- and fourth-level TBUs).

As for micron particle deposition, impaction is the dominant deposition mechanism at large airways (say, bifurcation unit B1–B3) so that depositions mainly occur around the carinal ridges (see Figs. 5 and 6). However, at medium to small sized airways (say, bifurcation units B7–B9 and B13–B15), sedimentation cannot be neglected, and the deposition patterns change somewhat. In this case, many particles essentially settle on the tube wall which is normal to the gravity direction. At the same time, the presence of gravity and the gravity direction affect the maximum DEF-value in each bifurcation. In general, some particles which may directly land on the carinal ridges when considering impaction only, can be diverted. As a result, the maximum DEF-values may decrease due to gravitational sedimentation. Specifically, the maximum DEF-values may reduce one order of magnitude (e.g., from about 1450 in B1–B3 to 340 in B7–B9 and 190 in B13–B15 as shown in Fig. 6) with much broader distribution of micron particles due to gravitational settling. Furthermore, the carinal ridges are not the unique deposition "hot spots" anymore; in fact, the entire airway surfaces which are normal to the gravity direction may become high-deposition regions. The location of bifurcation units, airway rotation and particle size may have significant effects on the maximum DEF-values for micron particles (Figs. 5 and 6).

In general, the maximum DEF-values range from the order of 10^2–10^3 for micron particles, which indicates that some local cells may receive hundreds times higher doses than the average values. Such extremely high local DEFs, i.e., "hot spots", for

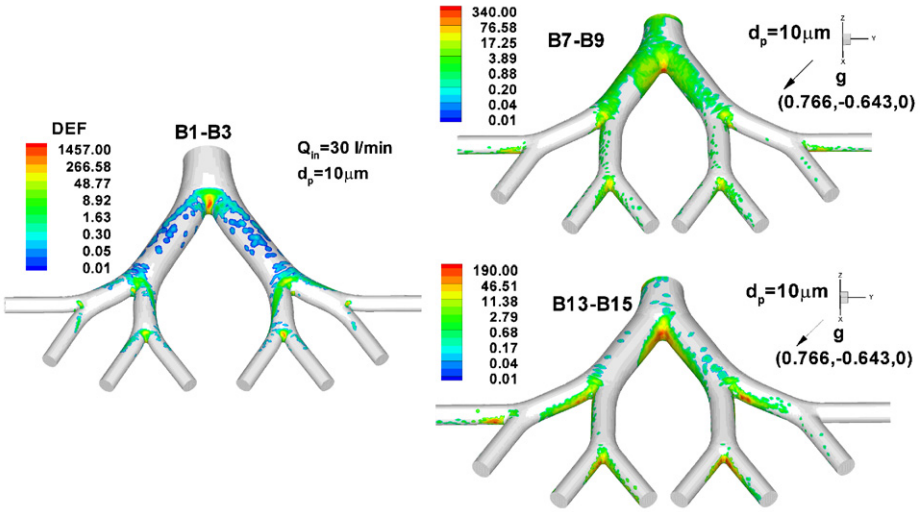

Fig. 6. Distributions of particle deposition enhancement factor (DEF) ($Q = 30$ L/min and $d_p = 10\,\mu$m). The mean areas of the surface element for calculating DEF are 0.2 mm^2, 0.012 mm^2 and 3×10^{-3} mm^2 for airway units B1–B3, B7–B9 and B13–B15, respectively.

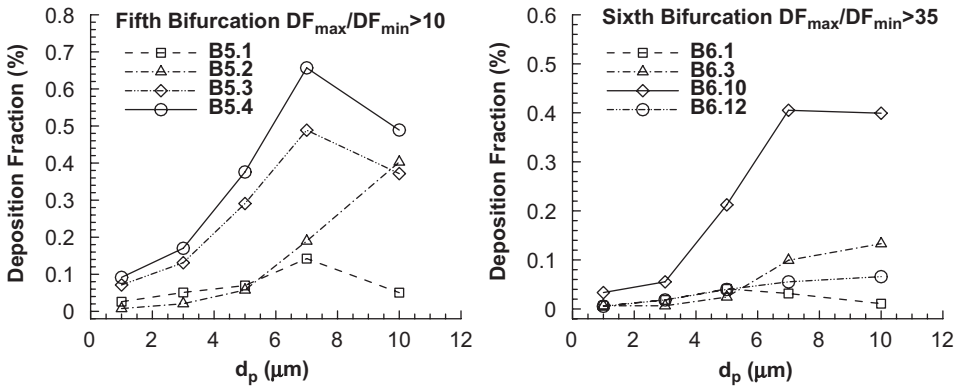

Fig. 7. Variations of local deposition fractions for micron particles ($Q = 30$ L/min).

micron particles indicates the possibility of local pathological changes in bronchial airways, such as the formation of lung tumors (Balashazy et al., 2003).

5.3. Variations of local DF and impact of airway rotation

5.3.1. Variations of local DFs

Variations of the total DFs for all parallel bifurcations as a function of particle size and level of the bifurcation "in series" were discussed in Section 5.1 (see Figs. 3 and 4). However, affected by the asymmetric flow rates at the outlets of each bifurcation unit as well as different parallel tubes, the local DFs may be quite different among parallel bifurcations with the same "serial number". Fig. 7 depicts the variations of local DFs as a function of particle size for micron particles in selected individual bifurcations, which feature the highest, lowest and medium depositions. Clearly, variations of DFs vs. micron-particle size are more complicated, because DFs may decrease for some large micron particles in some bifurcations due to the effects of upstream deposition and local air/particle transport. The local DF-values among individual parallel bifurcations may differ greatly; for example, the ratios of DF_{max}/DF_{min} may be larger than 10 for parallel bifurcations B5, while the ratios can be greater than 35 for the sixth-level bifurcations. It should be noted that the deposition in some small bifurcations (say, after B6) can be as low as zero when there are no incoming particles due to the extensive, asymmetric upstream depositions; hence, the ratio of DF_{max}/DF_{min} tends to be infinite in this case. All of these large differences among parallel bifurcations can be attributed mainly to the highly varying particle distributions at the inlets of specific bifurcations.

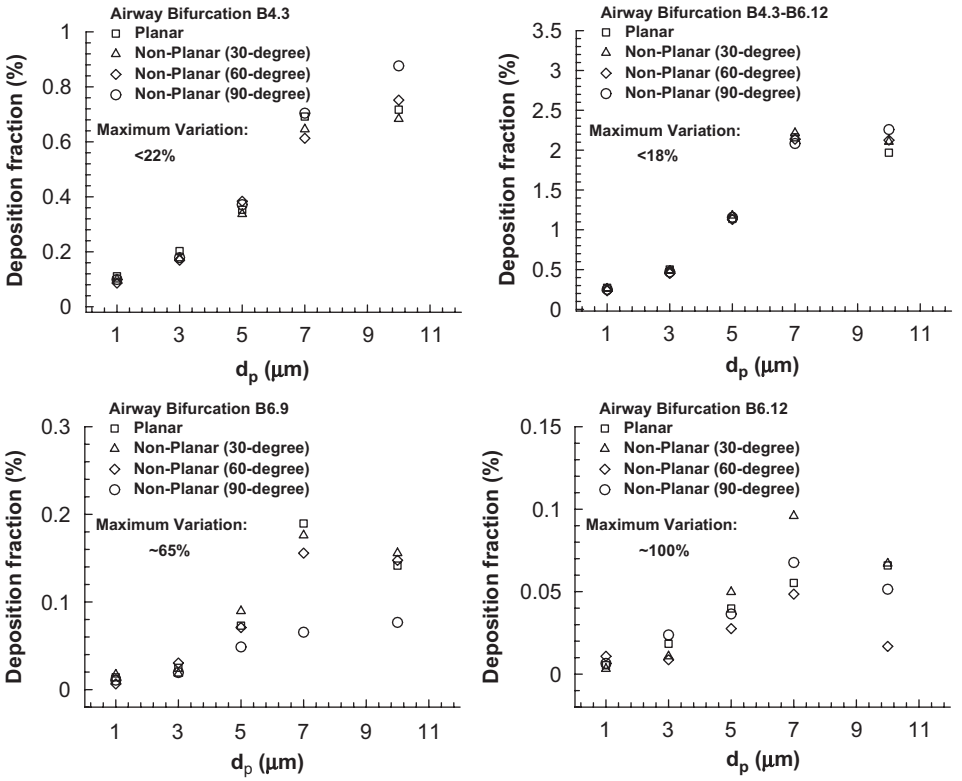

Fig. 8. Impact of airway rotation on micron particle deposition ($Q = 30$ L/min).

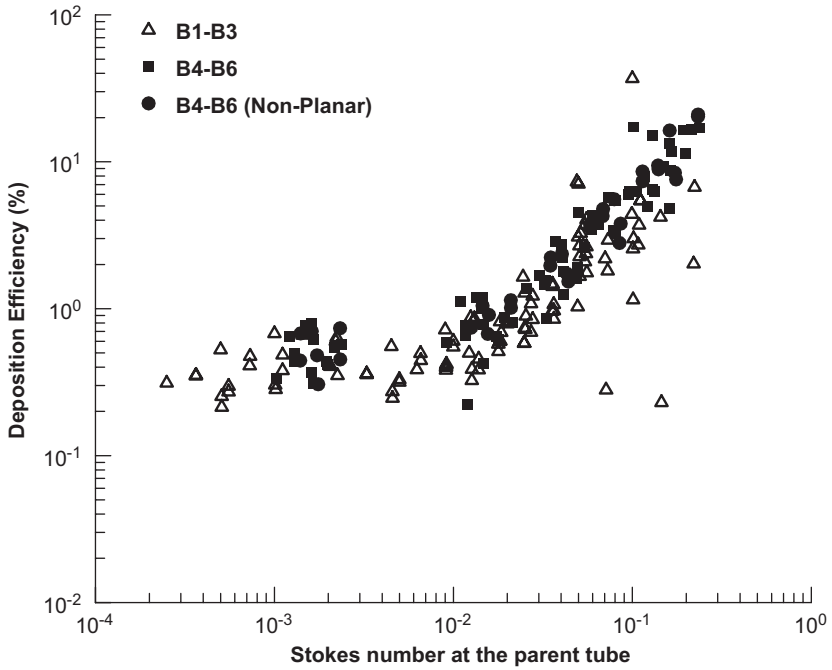

Fig. 9. Variations of bifurcation deposition efficiency of micron particles as a function of Stokes number. All data points are for cases of both $Q = 15$ and 30 L/min. The data for non-planar geometries are the combinations of three rotation angles (i.e., 30°, 60°, and 90° rotation).

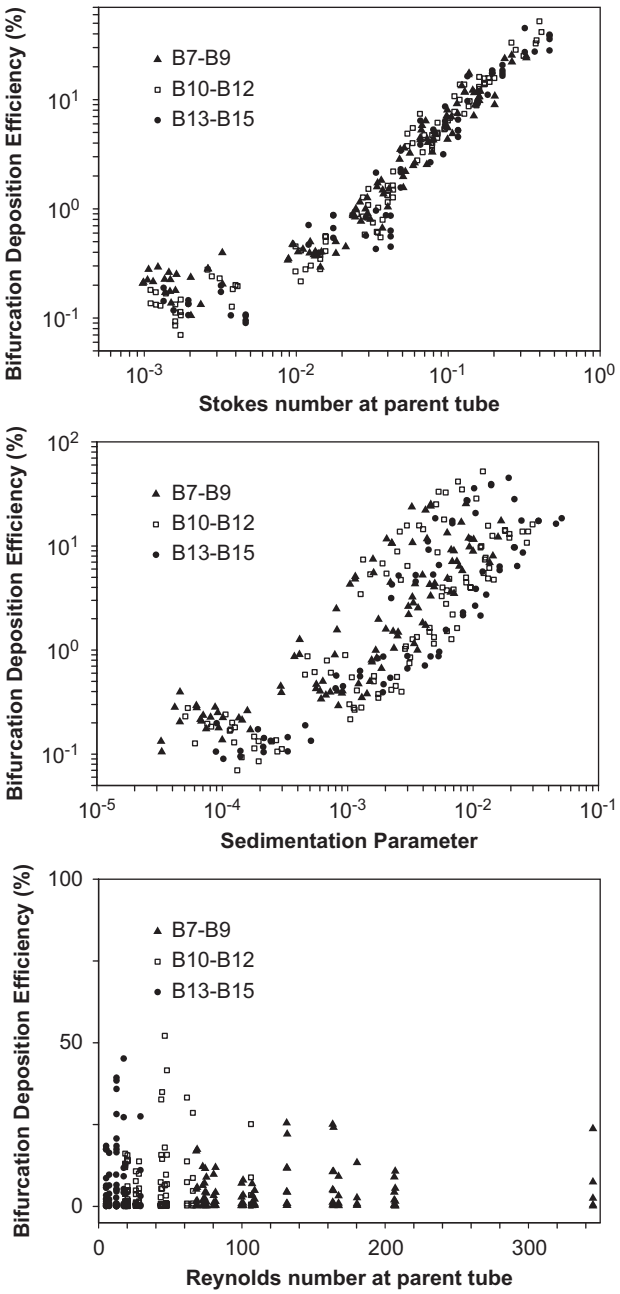

Fig. 10. Variations of bifurcation deposition efficiency of micron particles as a function of Stokes number, sedimentation parameter, and Reynolds number. All data points are for cases of both $Q = 15$ and 30 L/min.

5.3.2. Impact of airway rotation

The effects of non-planar geometries on particle transport and deposition patterns have been demonstrated in the previous sections (see Fig. 5). The impact of airway rotation on local DFs of micron particles in some selected bifurcations are given in Fig. 8. As expected, rotations of airway bifurcation may have a significant impact on distal bifurcations (say, B6.9 and B6.12) rather than the proximal ones (say, B4.3). The maximum variation of local DFs due to non-planar geometry effects ranges from 18% to 100% for micron particles. This may also imply that the flow history (i.e., local, incoming particle distributions and airflow structure) has a more significant effect on local DF-values than flow development and particle motion in local bifurcations caused by non-planar geometry. The variations of local inlet air/particle distributions can generate differences exceeding 35 times in local DFs among parallel bifurcations.

As shown in Fig. 8, the impact of airway rotation angle is complicated. For example, for micron particles in B6.9, the "30° rotation" case shows a maximum deposition for 1, 3, 5 and 10 μm particles, but the "90° rotation" may maximize the deposition of 7 μm particles. The situation may completely change in airway bifurcation B6.12.

5.4. Particle DEs and correlations

As mentioned, the development of deposition equations is crucial for swift, easy-to-execute assessments. The single correlation for micron particle DE is very difficult; because, as shown in Figs. 9 and 10, the DE-values are very scattered. Ignoring the geometric effects, the DE should be a function of both Stokes number and Reynolds number for the large airways, say, first to sixth bifurcation. The DE at small airways may be mainly a function of Stokes number, sedimentation parameter ($\gamma = (\nu_{\text{settling}}/U)(L/D)\cos\varphi$), and Reynolds number. Clearly, the DE usually increases with an increasing Stokes number due to impaction and an increasing sedimentation parameter because of gravitational settling (Fig. 10). The effect of Reynolds number on DE is somewhat complicated (Fig. 10). As the Reynolds number increases, the DE due to impaction may increase, but the DE due to sedimentation may decrease. Additional data points need to be obtained to generate good DE-correlations for micron particles.

6. Conclusions

This paper presents the first comprehensive attempt to compute micron particle transport in a 16-generation model of the human tracheobronchial region. Based on the experimentally validated computer simulation results, the following conclusions can be drawn:

(1) Surprisingly, simulated inspiratory deposition fractions for the *entire* tracheobronchial region (say, G0–G15) with repeated TBUs in parallel and in series agree rather well with those calculated using analytical/semi-empirical expressions. However, the predicted particle-deposition fractions based on such analytical formulas differ greatly from the present simulation results for most *local* bifurcations, due to the effects of local geometry and resulting local flow features and particle distributions. Clearly, the effects of realistic geometries, flow structures and particle distributions in different individual bifurcations accidentally cancel each other so that the simulated deposition efficiencies during inspiration in a relatively large airway region may agree quite well with those obtained from analytical expressions. Furthermore, with the lack of local resolution, analytical models do not provide any physical insight to the air–particle dynamics in the tracheobronchial region.
(2) The maximum deposition enhancement factors (DEF) may be in the order of 10^2 to 10^3 for micron particles in the tracheobronchial airways, implying potential health effects when the inhaled particles are toxic.
(3) The presence of sedimentation for micron particles in lower bronchial airways may change the local impaction-based deposition patterns seen for larger airways and hence reduces the maximum DEF values.
(4) Rotation of an airway bifurcation cause a significant impact on distal bifurcations rather than on the proximal ones. Such geometric effects are minor when compared to the effects of airflow and particle transport/deposition history, i.e., upstream effects.
(5) Future work will consider the effects of realistic airway geometries (e.g., asymmetry), unsteady flow conditions and particle characteristics (e.g., hygroscopicity, non-sphericity, etc.).

Acknowledgements

This effort was sponsored by the Air Force Office of Scientific Research, Air Force Material Command, USAF, under Grant number FA9550-07-1-0461 (Dr. Walt Kozumbo, Program Manager) NSF-grant CBET-0834054 (Dr. Marc S. Ingber, Program Director), and the US Environmental Protection Agency (Dr. C.S. Kim, Program Monitor). The US Government is authorized to reproduce and distribute reprints for governmental purposes notwithstanding any copyright notation thereon. The use of both CFX software from ANSYS Inc. (Canonsburg, PA) and IBM Linux Cluster at the High Performance Computing Center at North Carolina State University (Raleigh, NC) are gratefully acknowledged as well.

Disclaimer

The views and conclusions contained herein are those of the authors and should not be interpreted as necessarily representing the official policies or endorsements, either expressed or implied, of the Air Force Office of Scientific Research, the National Science Foundation, or the US Environmental Protection Agency.

References

ANSYS Inc. (2006). *Ansys—CFX solver theory guide*. Canonsburg, PA.
Asgharian, B., Hofman, W., & Bergmann, R. (2001). Particle deposition in a multiple-path model of the human lung. *Aerosol Science and Technology*, *34*(4), 332–339.

Balashazy, I., Hofmann, W., & Heistracher, T. (2003). Local particle deposition patterns may play a key role in the development of lung cancer. *Journal of Applied Physiology*, *94*(5), 1719–1725.
Chan, T. L., & Lippmann, M. (1980). Experimental measurements and empirical modeling of the regional deposition of inhaled particles in humans. *American Industrial Hygiene Association Journal*, *41*(6), 399–408.
Choi, J. I., & Kim, C. S. (2007). Mathematical analysis of particle deposition in human lungs: An improved single path transport model. *Inhalation Toxicology*, *19*(11), 925–939.
Clift, R., Grace, J. R., & Weber, M. E. (1978). *Bubbles, drops, and particles*. New York: Academic Press.
Comer, J. K., Kleinstreuer, C., & Zhang, Z. (2001). Flow structures and particle deposition patterns in double-bifurcation airway models. Part 1: Air flow fields. *Journal of Fluid Mechanics*, *435*, 25–54.
Emmett, P. C., Aitken, R. J., & Hannan, W. J. (1982). Measurements of the total and regional deposition of inhaled particles in the human respiratory-tract. *Journal of Aerosol Science*, *13*(6), 549–560.
Foord, N., Black, A., & Walsh, M. (1978). Regional deposition of 2.5–7.5 μm diameter inhaled particles in healthy male non-smokers. *Journal of Aerosol Science*, *9*, 343–357.
Goo, J., & Kim, C. S. (2003). Theoretical analysis of particle deposition in human lungs considering stochastic variations of airway morphology. *Journal of Aerosol Science*, *34*(5), 585–602.
Gosman, A. D., & Ioannides, E. (1981). Aspects of computer simulation of liquid-fueled combustors. *Journal of Energy*, *7*, 482–490.
International Commission on Radiolocial Protection (ICRP) (1994). Human respiratory tract model for radiological protection. *Annals of the ICRP*, ICRP Publication 66, New York: Elsevier.
Kim, C. S., & Hu, S. C. (2006). Total respiratory tract deposition of fine micrometer-sized particles in healthy adults: Empirical equations for sex and breathing pattern. *Journal of Applied Physiology*, *101*(2), 401–412.
Kim, C. S., & Jaques, P. A. (2004). Analysis of total respiratory deposition of inhaled ultrafine particles in adult subjects as various breathing patterns. *Aerosol Science and Technology*, *38*(6), 525–540.
Kim, J., Moin, P., & Moser, R. (1987). Turbulence statistics in fully-developed channel flow at low Reynolds-number. *Journal of Fluid Mechanics*, *177*, 133–166.
Kleinstreuer, C. (2003). *Two-phase flow: Theory and applications*. New York: Taylor & Francis.
Kleinstreuer, C. (2006). *Biofluid dynamics: Principles and selected applications*. Boca Raton, FL: CRC Press.
Kleinstreuer, C., & Zhang, Z. (2003). Laminar-to-turbulent fluid–particle flows in a human airway model. *International Journal of Multiphase Flow*, *29*(2), 271–289.
Kleinstreuer, C., & Zhang, Z. (2008). An adjustable triple-bifurcation unit model for air–particle flow simulations in human tracheobronchial airways. *ASME Journal of Biomechanical Engineering*, in press.
Kleinstreuer, C., Zhang, Z., & Donohue, J. F. (2008). Targeted drug-aerosol delivery in the human respiratory system. *Annual Review of Biomedical Engineering*, *10*, 195–220.
Kleinstreuer, C., Zhang, Z., & Kim, C. S. (2007). Combined inertial and gravitational deposition of microparticles in small model airways of human respiratory system. *Journal of Aerosol Science*, *38*, 1047–1061.
Koblinger, L., & Hofmann, W. (1990). Monte-Carlo modeling of aerosol deposition in human lungs. 1: Simulation of particle-transport in a stochastic lung structure. *Journal of Aerosol Science*, *21*(5), 661–674.
Li, Z., Kleinstreuer, C., & Zhang, Z. (2007). Particle deposition in the human tracheobronchial airways due to transient inspiratory flow patterns. *Journal of Aerosol Science*, *38*(6), 625–644.
Lippmann, M. (1977). Regional deposition of particles in the human respiratory tract. In D. H. K. Lee et al. (Eds.), *Handbook of physiology—reaction to environmental agents* (pp. 213–232). Bethesda, MD: American Physiology Society.
Longest, P. W., Kleinstreuer, C., & Buchanan, J. R. (2004). Efficient computation of micro-particle dynamics including wall effects. *Computers & Fluids*, *33*(4), 577–601.
Longest, P. W., & Xi, J. X. (2007). Computational investigation of particle inertia effects on submicron aerosol deposition in the respiratory tract. *Journal of Aerosol Science*, *38*(1), 111–130.
Macinnes, J. M., & Bracco, F. V. (1992). Stochastic particle dispersion modeling and the tracer-particle limit. *Physics of Fluids A—Fluid Dynamics*, *4*(12), 2809–2824.
Matida, E. A., Finlay, W. H., Lange, C. F., & Grgic, B. (2004). Improved numerical simulation of aerosol deposition in an idealized mouth–throat. *Journal of Aerosol Science*, *35*(1), 1–19.
Matida, E. A., Nishino, K., & Torii, K. (2000). Statistical simulation of particle deposition on the wall from turbulent dispersed pipe flow. *International Journal of Heat and Fluid Flow*, *21*(4), 389–402.
National Council on Radiation Protection and Measurements (NCRP) (1997). *Deposition, retention, and dosimetry of inhaled radioactive substances*. Report no. 125, National Council on Radiation Protection and Measurements, Bethesda, MD.
National Institute for Public Health and the Environment (RIVM) (2002). *Multiple path particle dosimetry model (MPPD v 1.0): A model for human and rat airway particle dosimetry*. RIVA report 650010030, Bilthoven, The Netherlands.
Nowak, N., Kakade, P. P., & Annapragada, A. V. (2003). Computational fluid dynamics simulation of airflow and aerosol deposition in human lungs. *Annals of Biomedical Engineering*, *31*(4), 374–390.
Tian, L., & Ahmadi, G. (2007). Particle deposition in turbulent duct flows—comparisons of different model predictions. *Journal of Aerosol Science*, *38*(4), 377–397.
Varghese, S. S., & Frankel, S. H. (2003). Numerical modeling of pulsatile turbulent flow in stenotic vessels. *Journal of Biomechanical Engineering—Transactions of the ASME*, *125*(4), 445–460.
Wang, Y., & James, P. W. (1999). On the effect of anisotropy on the turbulent dispersion and deposition of small particles. *International Journal of Multiphase Flow*, *25*(3), 551–558.
Weibel, E. R. (1963). *Morphometry of the human lung*. New York: Academic Press.
Wilcox, D. C. (1998). *Turbulence modeling for CFD LA*. Canada, CA: DCW Industries, Inc.
Zhang, Z., & Kleinstreuer, C. (2002). Transient airflow structures and particle transport in a sequentially branching lung airway model. *Physics of Fluids*, *14*(2), 862–880.
Zhang, Z., & Kleinstreuer, C. (2003a). Low-Reynolds-number turbulent flows in locally constricted conduits: A comparison study. *AIAA Journal*, *41*(5), 831–840.
Zhang, Z., & Kleinstreuer, C. (2003b). Species heat and mass transfer in a human upper airway model. *International Journal of Heat and Mass Transfer*, *46*(25), 4755–4768.
Zhang, Z., & Kleinstreuer, C. (2004). Airflow structures and nano-particle deposition in a human upper airway model. *Journal of Computational Physics*, *198*(1), 178–210.
Zhang, Z., Kleinstreuer, C., Donohue, J. F., & Kim, C. S. (2005). Comparison of micro- and nano-size particle depositions in a human upper airway model. *Journal of Aerosol Science*, *36*(2), 211–233.
Zhang, Z., Kleinstreuer, C., & Kim, C. S. (2002). Gas–solid two-phase flow in a triple bifurcation lung airway model. *International Journal of Multiphase Flow*, *28*(6), 1021–1046.